Swarm IPIR Validation Report

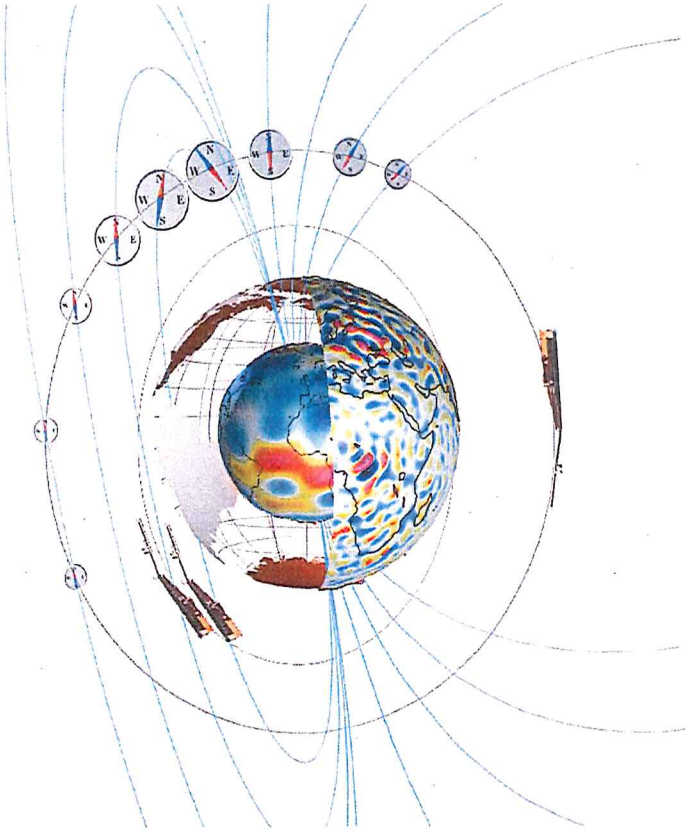

Doc. no: SW-TN-UiO-GS-004, Rev: 1A, 01 September 2018

Prepared:

Yaqi Jin

Yaqi Jin Date 01 Sept. 2018

Scientist

Prepared:

Chao Xiong

Chao Xiong Date 01 Sept. 2018

Scientist

Approved:

Wojciech J. Miloch Date 01 Sept. 2018

Project Manager

Record of Changes

Reason	Description	Rev	Date
Initial vers.	Released	1 dA	10 June 2018
Updated IPIR index.	Released	2 dA	28 August 2018
Final version	Updated description of the IPIR index, formatting corrections, correction of Rev. number.	1A	01 Sept. 2018

Table of Contents

1 Introduction

1.1 Scope and applicability

This document comprises the Swarm Level 2 (L2) IPIR product Validation Report (VR) document for the Swarm Data, Innovation and Science Cluster (Swarm DISC) consortium in response to the requirements of [AD-1]. Swarm-IPIR uses the following products [AD-4]:

- EFIx_PL_1B – 2Hz data from the Electrical Field Instrument (EFI).
- TECxTMS_2F – TEC data derived from onboard GPS.
- AOBxFAC_2F – Auroral Oval Boundaries (AOB) using the Field-Aligned Current (FAC) method.
- IBIxTMS_2F, IBI: Ionospheric Bubble Index.
- Polar Cap Products (PCP).

The Swarm-IPIR Product Definition document [AD-4] is available in the SVN folder: https://smart-svn.space-center.dk/svn/smart/SwarmDISC/DISC_Projects/ITT1_4_ionospheric_irregularities/Deliverables/.

Current or updated version of this document is available in the SVN folder: https://smart-svn.space-center.dk/svn/smart/SwarmDISC/DISC_Projects/ITT1_4_ionospheric_irregularities/Deliverables/.

2 Applicable and Reference Documentation

2.1 Applicable Documents

The following documents are applicable to the definitions within this document.

[AD-1] SW-SW-DTU-GS-114, rev 1 Statement of Work for Swarm DISC ITT 1.4 “Ionospheric irregularities and fluctuations based on Swarm data”

[AD-2] IPIR-Swarm-IPIR-12017 – Ionospheric Plasma IRregularities characterised by the Swarm satellites.

[AD-3] https://earth.esa.int/web/guest/missions/esa-eo-missions/swarm/data-handbook

[AD-4] SW-TN-UiO-GS-001, Swarm-IPIR Product Definition.

[AD-5] SW-TN-UiO-GS-003, Swarm-IPIR Description of the Processing Algorithm.

2.2 Reference Documents

The following documents contain supporting and background information to be taken into account during the activities specified within this document.

[RD-1] SW-TN-UiO-GS-003, Swarm-IPIR Description of the Processing Algorithm.

[RD-2] Crowley, G., A. J. Ridley, D. Deinst, S. Wing, D. J. Knipp, B. A. Emery, F. Foster, R. Heelis, M. Hairston, and B. W. Reinisch (2000), Transformation of high-latitude ionospheric F region patches into blobs during the March 21, 1990, storm, J. Geophys. Res., 105, 5215–5230, doi:10.1029/1999JA900357.

[RD-3] Yeh K.-Ch. And Liu, Ch.-H. (1982), Radio Wave Scintillations in the Ionosphere, Proc. IEEE 70, 324-360.

2.3 Abbreviations

Acronym ***or abbreviation***	***Description***
AOB	Auroral Oval Boundaries
DISC	The Data, Innovation and Science Cluster
DPA	Description of the Processing Algorithm
ESA	European Space Agency
FAC	Field-Aligned Current
GFZ	The Helmholtz Centre Potsdam - GFZ German Research Centre for Geosciences, DE
L1b	Level 1b (satellite data)
L2	Level 2 (satellite data)
MLAT	Magnetic Latitude
SVN	SVN Repository with server located at DTU. Presently, the following URLs apply: https://smart-svn.spacecenter.dk/svn/smart/SwarmDISC/DISC_Projects/ITT1_4_ionospheric_irregularities/Deliverables/
Swarm	Constellation of 3 ESA satellites, https://earth.esa.int/web/guest/missions/esa-operational-eo-missions/swarm
TBD	To Be Defined
UiO	The University of Oslo, Oslo, Norway
GISTM	GNSS Ionospheric Scintillation and TEC Monitor

3 Rationale and background

This document provides a validation report for the IPIR-product, which characterises plasma density fluctuations and irregularities encountered by Swarm in terms of their spatial occurrence and amplitudes. This can be analysed relative to the local plasma conditions, i.e., to the local background. IPIR also relates the fluctuations to the ionospheric current system and variations in the magnetic field, in order to relate these structures to dynamic phenomena in the ionosphere. Finally, it combines data from the GPS receivers, where TEC and ROT provide information on the extent of the structures in the direction towards GPS satellites.

The data is acquired from the following instruments onboard Swarm: Electric Field Instrument, which includes the Langmuir probe (LP) and Thermal Ion Imager (TII), magnetometers and GPS antennas. Location of instruments onboard Swarm is shown in Fig. 1.

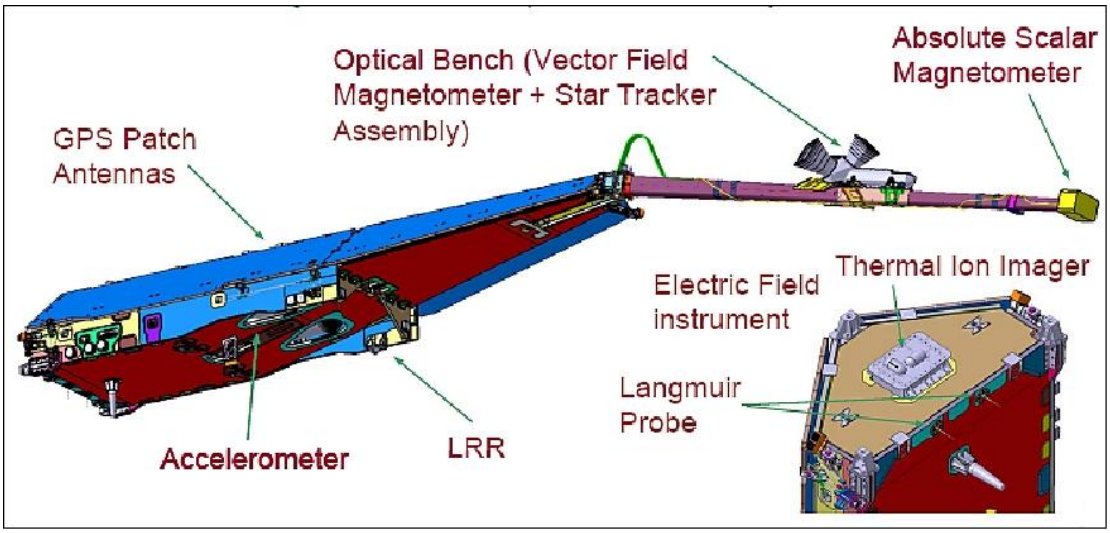

Fig. 1. Swarm satellite with its scientific instruments (Courtesy of ESA).

Based on Swarm data, in the IPIR product, we derive the following parameters, whose definition can be found in the Swarm-IPIR Description of the Processing Algorithm [RD-01]:

- Rate Of change of Density (ROD),
- Rate Of change of Density Index in 10 seconds (RODI10s),
- Rate Of change of Density Index in 20 seconds (RODI20s),
- filtered *Ne* fluctuations in 10 seconds (delta_Ne10s),
- filtered *Ne* fluctuations in 20 seconds (delta_Ne20s),
- filtered *Ne* fluctuations in 40 seconds (delta_Ne40s),
- *Ne* gradient in 100 km scale (Grad_Ne@100km),
- *Ne* gradient in 50 km scale (Grad_Ne@50km),
- *Ne* gradient in 20 km scale (Grad_Ne@20km),
- *Ne* gradient near the edge of a polar cap patch (Grad_Ne@PCP_edge),
- Rate of change of TEC (*ROT*),
- Rate of change of TEC index (*ROTI*).

In the report we compare the satellite derived data between different datasets and with data from selected ground stations with GNSS Ionospheric Scintillation and TEC Monitors (GISTMs). With these ground-based receivers we can monitor the following quantities:

- GPS phase and amplitude scintillation indices (σ_ϕ and S_4), minutely values,
- TEC along the receiver-satellite pair, minutely value,
- ROT and ROTI from the TEC data.

A typical set-up of the GISTM receiver is given in Fig. 2,

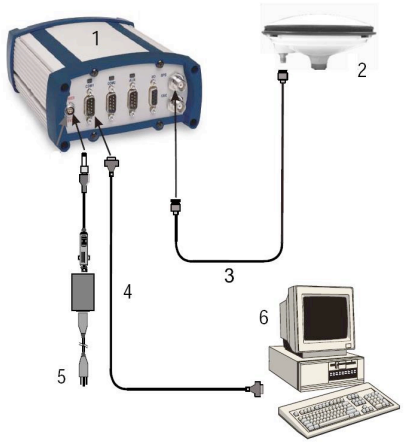

Fig. 2. Typical GISTM receiver consisting of 1) processing unit, 2) receiving antenna, 3-5) cables and interfaces, 6) computer.

IPIR includes several other parameters in the dataset, such as PCP-index, IBI-flag, *Te* (electron temperature), *Ne* (electron density), which have already been validated through a development of other products. In this VR we therefore focus on the new parameter ROD, and also TEC and ROT calculated onboard Swarm, as we can compare those to a different dataset. Derived quantities such as *Ne* fluctuations and gradients are derived from *Ne* using a standard approach as described in [RD-01], and thus cannot be directly compared with independent measurements of the same quantity.

4 Comparison of Swarm based measurments

As the first test we compare two independent measurements taken onboard Swarm satellites. Local electron density measurements are compared with the TEC measurements, which provide indication of the integrated electron density between the receiver and GNSS satellite. From Fig. 3, showing daily overview of data it is clear that both datasets are correlated positively. A closer inspection is given in Fig. 4, which shows that structures in two datasets are similar, indicating that irregularities in density can correspond to irregularities in TEC. Thus in Fig. 5 we present a comparison of ROD and ROT derived onboard Swarm and note a satisfactory agreement. To quantify the agreement, we use RODI and ROTI and calculate the correlation coefficient between those two. In general, there is a good correlation between the two parameters for the disturbed plasma conditions. The stronger the variations in density, the better the agreement between the two datasets.

Fig. 3 Daily overview of TEC and Ne data measured by Swarm.

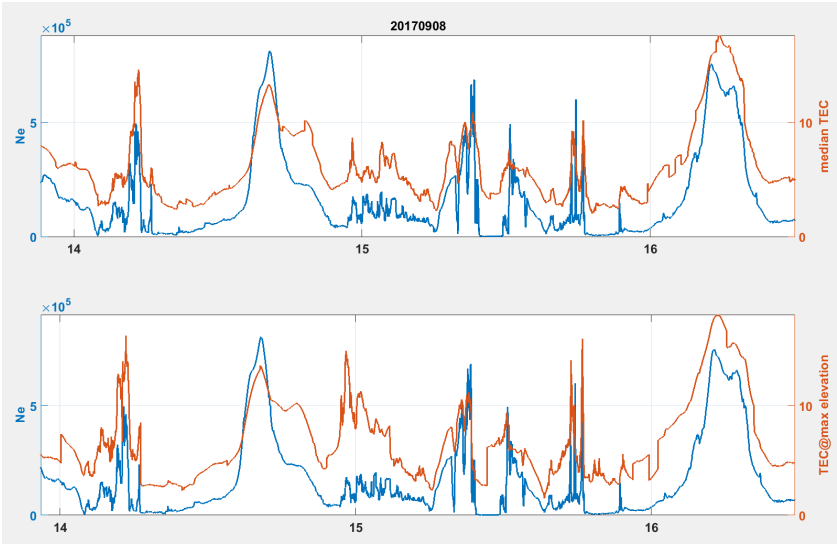

Fig. 4. As in Fig. 3 but a zoom in for 2.5 hours of data.

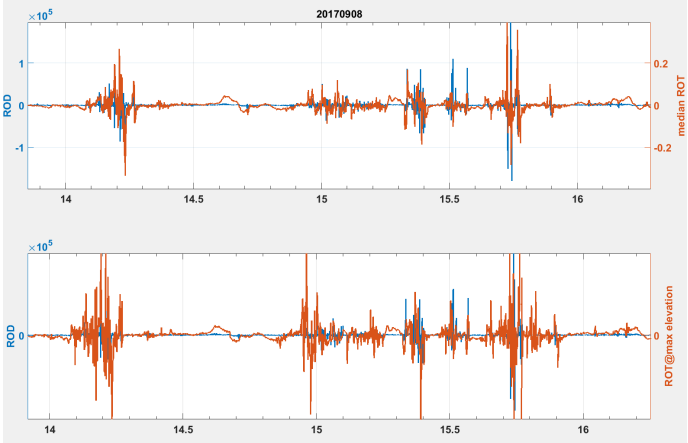

Fig. 5. ROD and ROT comparison during 2.5 hours corresponding to Fig. 4.

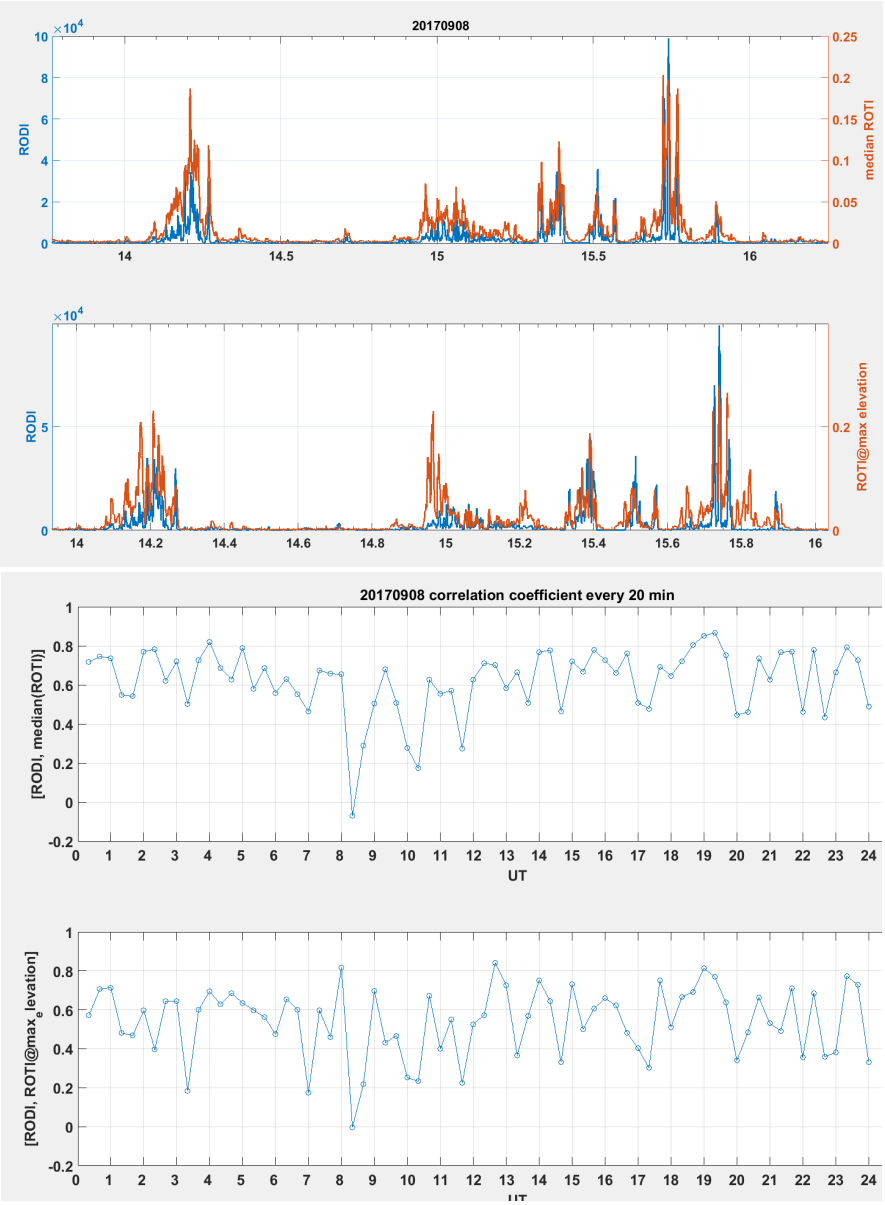

Fig. 6. RODI and median ROTI as well as correlation coefficient between RODI and ROTI as a function of time.

5 Comparison with ground-based GPS scintillation receivers

5.1 Overview of GISTM receivers

We use 3 selected GISTM receivers to cover the polar cap, auroral and equatorial regions, as these are the regions of different characteristics characterised by different processes in the ionosphere. The locations together with their respective field-of-view are shown in Fig. 7. The locations of the host stations are given in Table 1. In the following, we will use only data from GPS satellites.

Site name	Location	(Latitude, Longitude)
NYA	Ny-Ålesund, Svalbard	(78.92°N, 11.93°E)
SKN	Skibotn, Norway	(69.43°N, 20.38°E)
SZT	ShenZhen, China	(22.6°N, 114.0°E)

Table 1. Locations of 3 GISTM receivers used for validation.

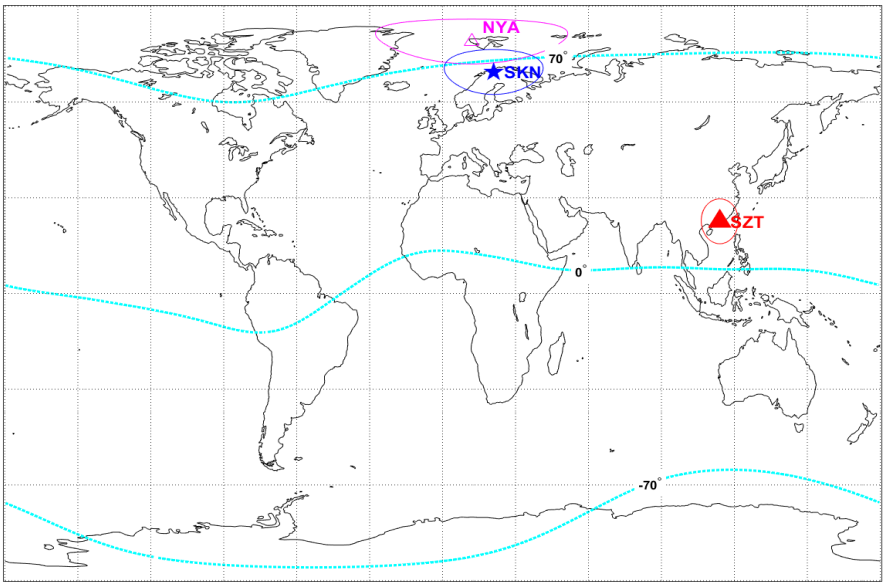

Fig. 7. Location of GISTM receivers presented in this validation report.

5.2 Conjunction with the polar cap station at Ny-Ålesund (NYA)

In order to compare IPIR products with ground-based GPS data, we need to find time intervals when the Swarm satellites pass over the field-of-view of the ground-based GPS receiver. To give a sense of the conjunction geometry, we show in Fig. 8 an example of the conjunction between the Swarm A and the ground-based GPS scintillation receiver at Ny-Ålesund on Feb. 9, 2015 at around 22 UT. The left panels in Fig. 8 show observations from Swarm A. For clarity of presentation, we did not plot all parameters from the IPIR dataset.

Fig. 8a-8b show the parameters derived from the electron density (*Ne*). The background electron density is derived by using a 35 percentile filter in a running window of 551 data points, which corresponds to a distance of about 2000 km travelled by the satellite (the sampling frequency being 2 Hz and the velocity of

the satellites being about 7.5 km/s). In order to show the detection of a polar cap patch, we also plot 2 times the background density in magenta as the polar cap patches are often defined as at least two times the background electron density in the polar cap [Crowley et al., 1996]. From the presented dataset we observe that one polar cap patch was detected by Swarm A around 22:02.35 UT. Worth noticing are NYA data from satellites PRN6 and PRN20, which correspond to second half of time interval presented for Swarm. ROT measured for both satellites shows relatively large variations, which one can directly relate to ROD, ROT, and even a small enhancement in the phase scintillation index.

To make the long-term statistics of the conjunction observation, we use data from September to December of 2014 at Ny-Ålesund. Fig. 9 show the scatter plots of VTEC from Ny-Ålesund versus VTEC and electron density from Swarm A. We only use data when the Swarm satellite passed over the field-of-view (indicated with a red circle in Fig. 8f) for more than 60 s. In the scatter plot, one circle in each plot represents one conjunction in the same manner as Fig. 8. It is clear that both density and VTEC measured from space show good correlation with the VTEC observation from ground. A linear fit is shown in each panel in a red line where the linear fit coefficient is shown on the top left of each panel. Thus, there is a good linear relationship between the two datasets.

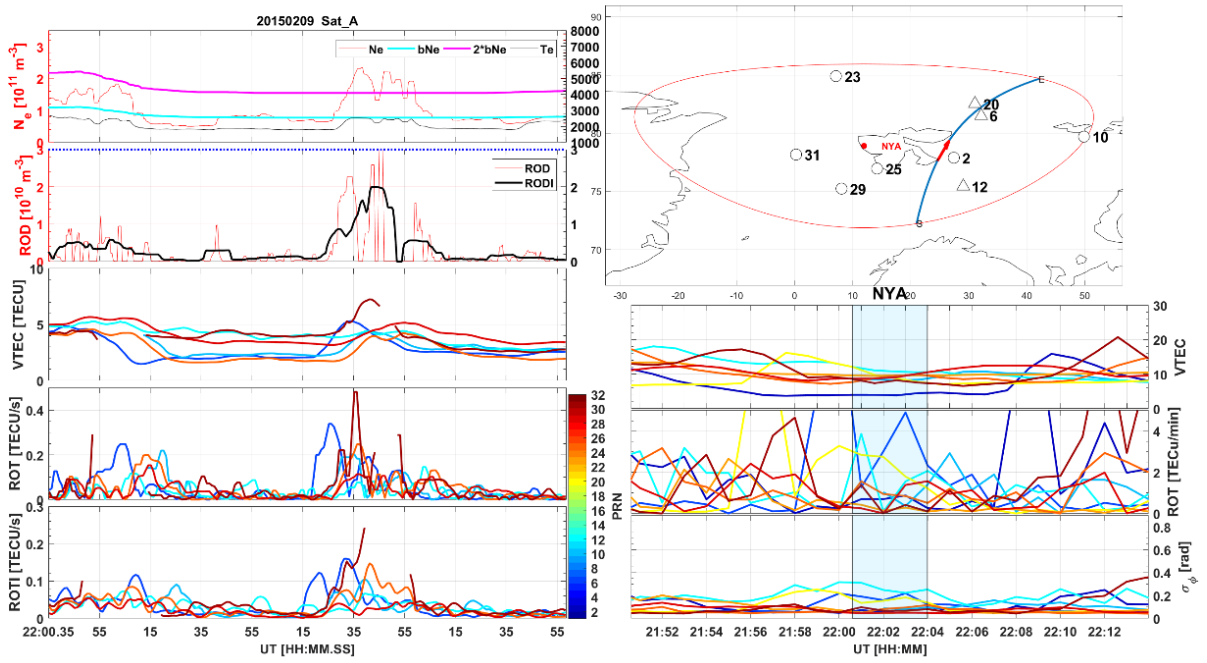

*Fig. 8. An example of the conjunction of Swarm A and the ground-based GPS scintillation receiver at Ny-Ålesund. (a-e) shows the data from Swarm A. (a) The electron density (Ne, red), background electron density (bNe, cyan), 2 times the background density (2*bNe, cyan), and electron temperature (Te, black). (b) The rate of change of density (ROD, absolute values) and RODI. (c) The GPS TEC data onboard Swarm. (d-e) The rate of change of TEC (ROT) and rate of change of TEC index (ROTI). The data from different GPS satellites are color-coded according to the PRN code in the colorbar on the right. (f) A map showing the field-of-view (red circle) of the GPS scintillation receiver at Ny-Ålesund (red dot), and the blue segment presents the Swarm orbit with an arrow showing the direction; the black circles and triangles show the piercing points of the GPS satellites tracked by the ground-based GPS receiver. (g-i) The GPS TEC, ROT and phase scintillation index (σ_ϕ) from the Ny-Ålesund GISTM receiver taking into account only GPS satellite data. The shaded area shows the time interval when Swarm A passes the field-of-view (red circle in panel f).*

Fig. 10 shows a comparison between ground-based measurements of the phase scintillation index (σ_ϕ) and the 4 selected parameters from Swarm A, namely RODI, ROTI, and the standard deviation of the electron density (std(*Ne*)) during the time interval when Swarm passes the field-of-view of Ny-Ålesund receiver, and the density gradient at 100 km scale. The irregularity parameters from Swarm are correlated with the ground-based phase scintillation strength, i.e., when RODI (ROTI, std(*Ne*), ∇Ne) increases, σ_ϕ increases as well. However, the relation is unlikely to be linear and therefore we do not make a linear fit as in Fig. 9.

Fig. 11 and Fig. 12 show the comparison between the ground-based GPS data (namely the amplitude scintillation index (S_4) and ROTI) and the Swarm datasets using the same format as Fig. 10. Both the amplitude scintillation index (S_4) and ROTI are loosely correlated with the Swarm derived irregularity parameters. This is to be expected, since S_4 is related to irregularities at scales of hundreds of meters, corresponding to a Fresnel scale [RD-03], while Swarm allows for detecting density gradients at km scales. Nevertheless, for large fluctuations in density observed by Swarm, we expect smaller scale fluctuations to be present as well, and thus we expect relationship between the two quantities.

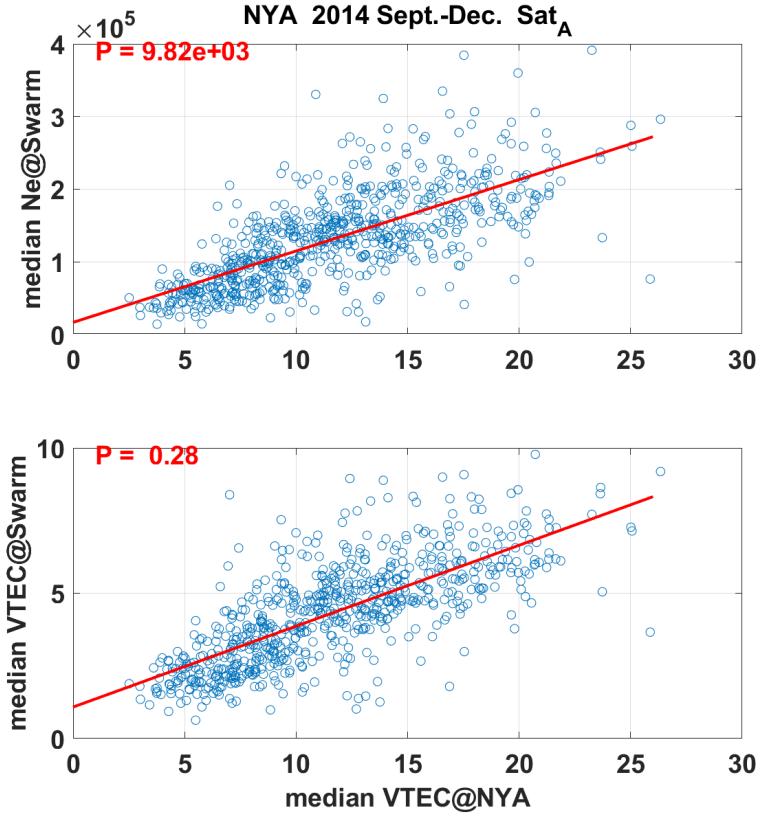

Fig. 9. Scatter plot of the VTEC from Ny-Ålesund versus VTEC and electron density from Swarm A. One circle in each plot represents one similar conjunction as the one in Fig. 8.

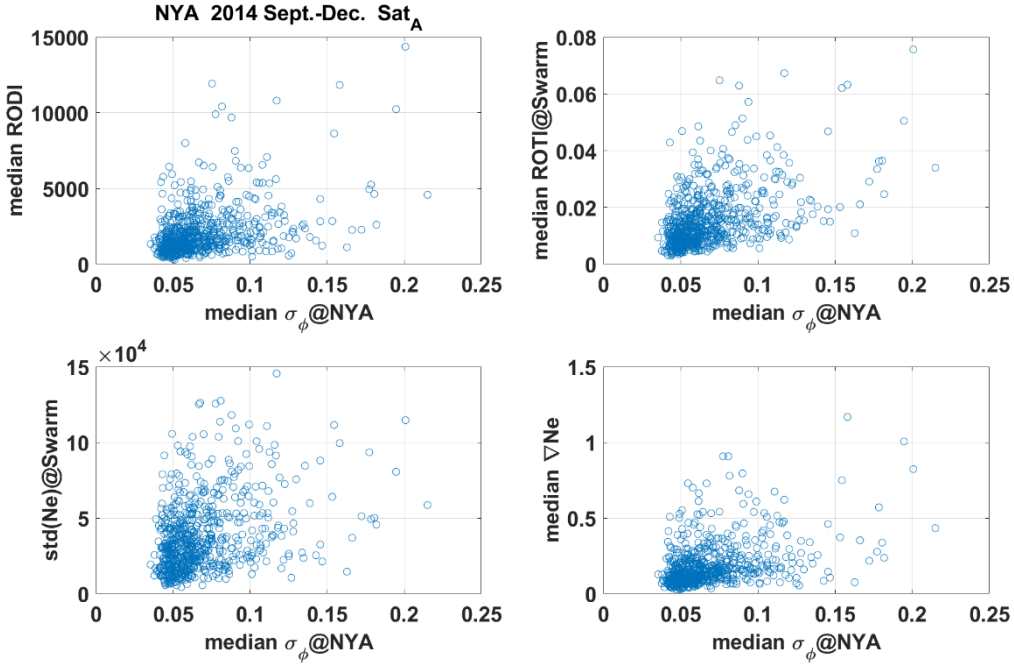

Fig. 10. Scatter plot of the phase scintillation index (σ_ϕ) from Ny-Ålesund versus selected parameters from Swarm A. Here one circle in each plot represents one conjunction in Fig. 8.

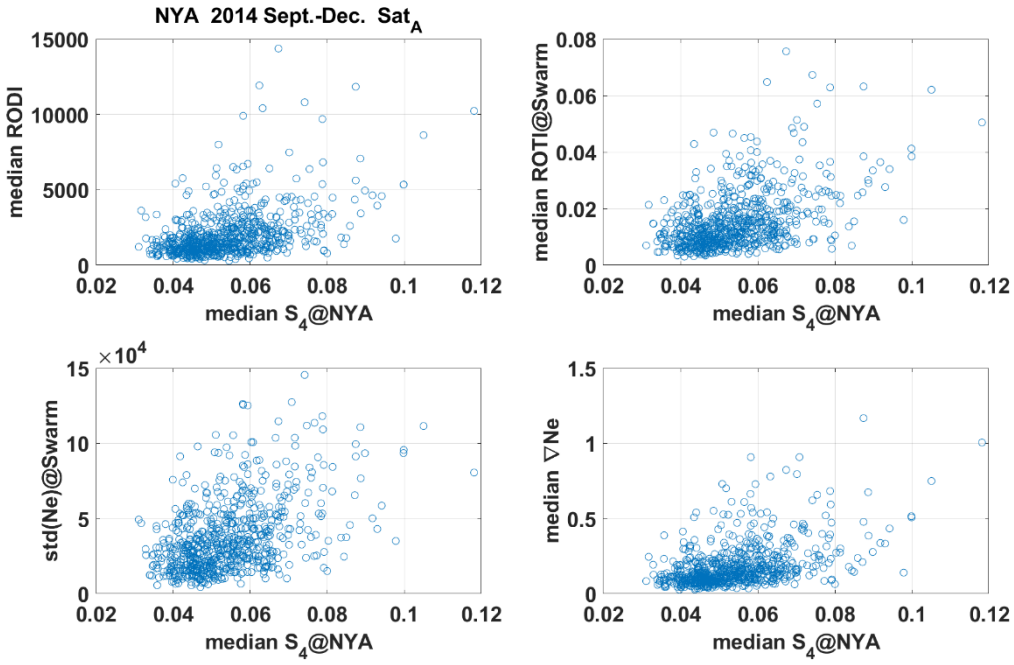

Fig. 11. Scatter plot of the amplitude scintillation index (S_4) from Ny-Ålesund station versus selected parameters from Swarm A.

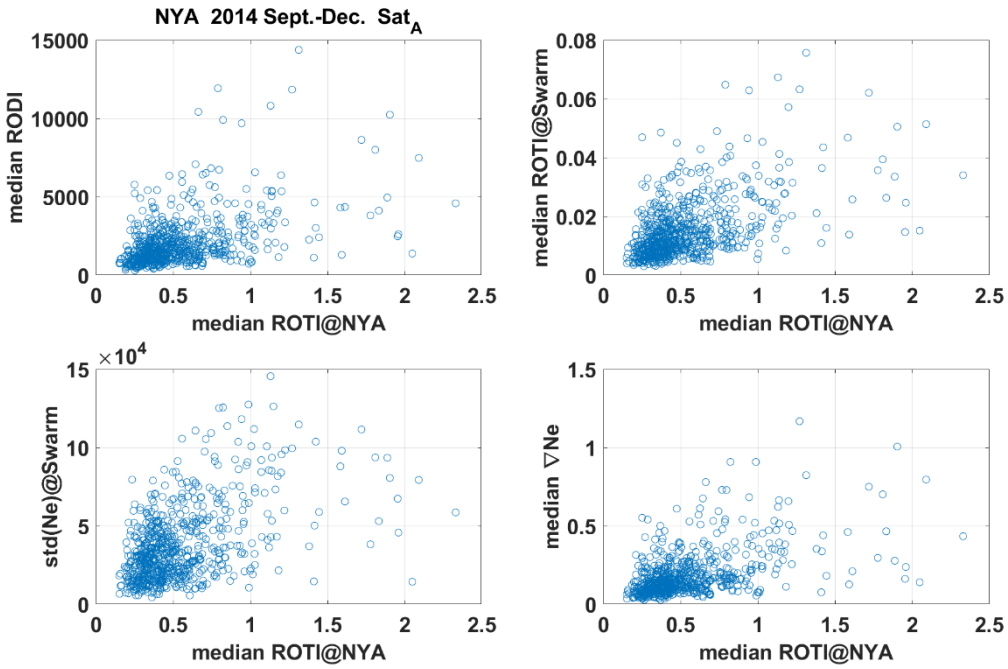

Fig. 12. Scatter plot of ROTI determined from GISTM at Ny-Ålesund station versus selected parameters from Swarm A.

5.3 Conjunction with the auroral station at Skibotn (SKN)

The GPS scintillation receiver at Skibotn is not continuously operated due to its remote location and maintenance issues. Fig. 13 shows operation times from 2014 to 2017. For comparison with Swarm, we use Skibotn data from Oct. 2014 to May 2015.

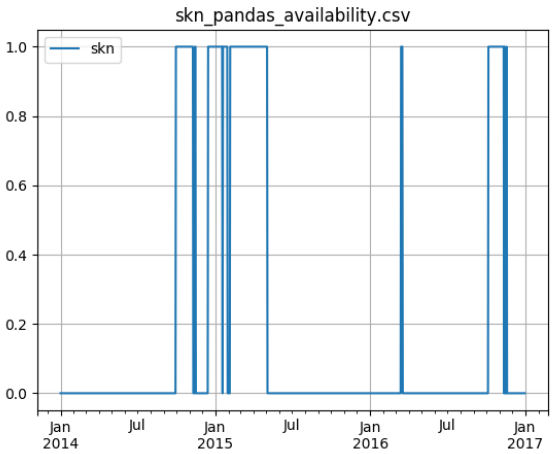

Fig. 13. Operation times of the Skibotn receiver: 1 indicates data available and 0 indicates no data.

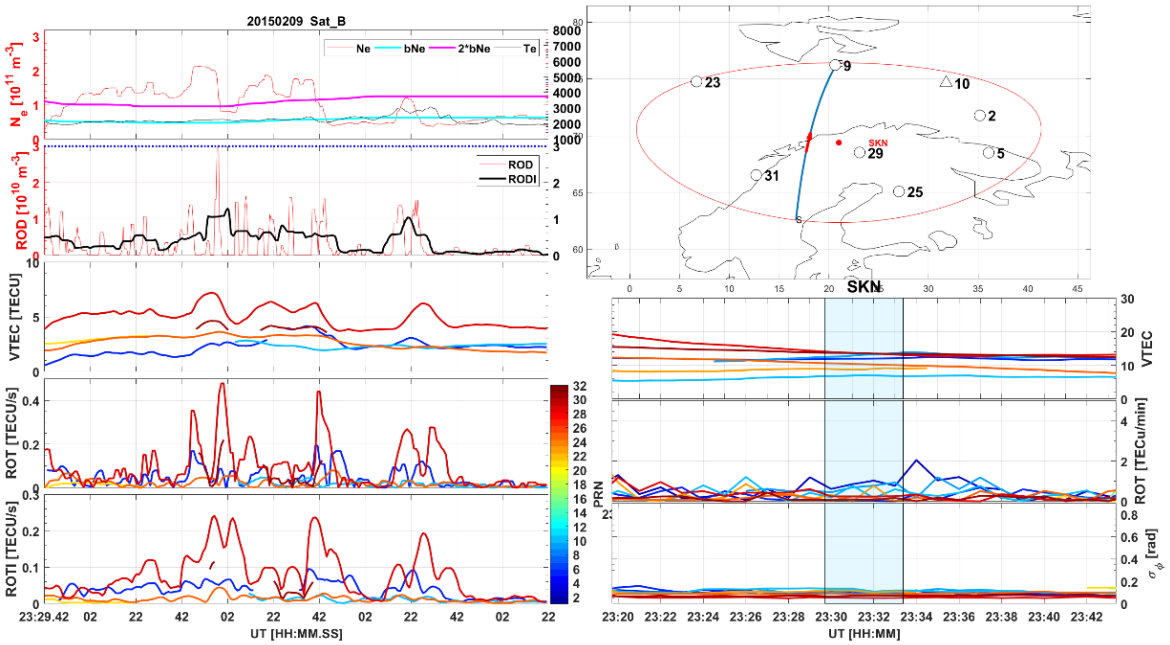

Fig. 14. Example of the conjunction of Swarm B and the ground-based GPS scintillation receiver at Skibotn. The figure is in the same format as Fig. 8.

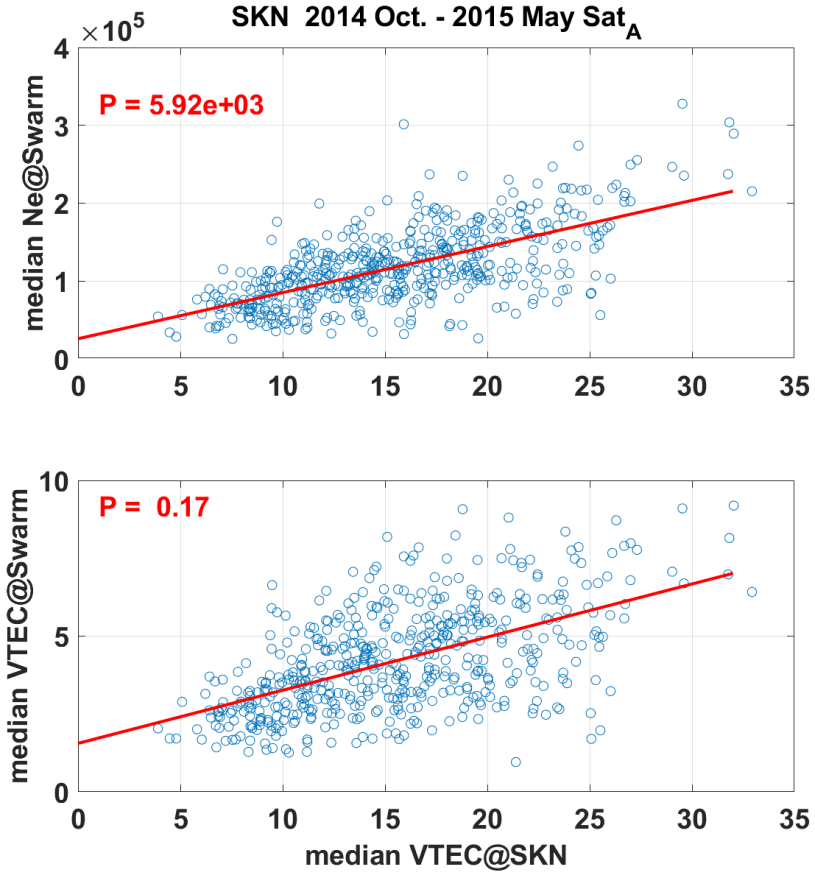

Fig. 15. Scatter plot of VTEC from Skibotn versus VTEC and electron density from Swarm A. One circle in each plot represents one similar conjunction as the one in Fig. 14.

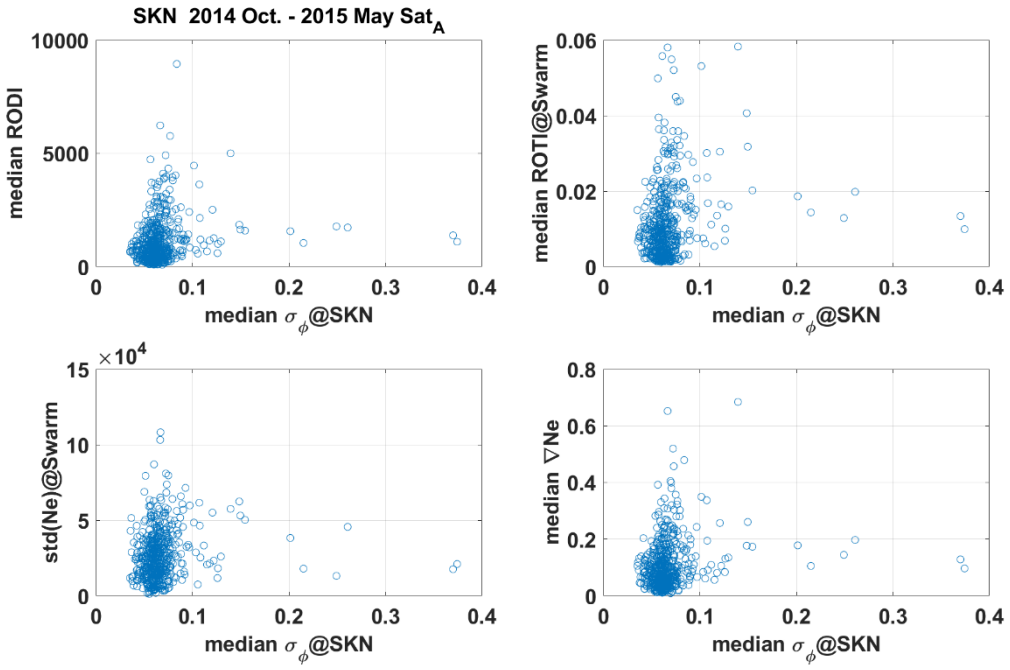

Fig. 16. Scatter plot of the phase scintillation index (σ_ϕ) from Skibotn versus selected parameters from Swarm A. Here one circle in each plot represents one conjunction similar to the one in Fig. 14.

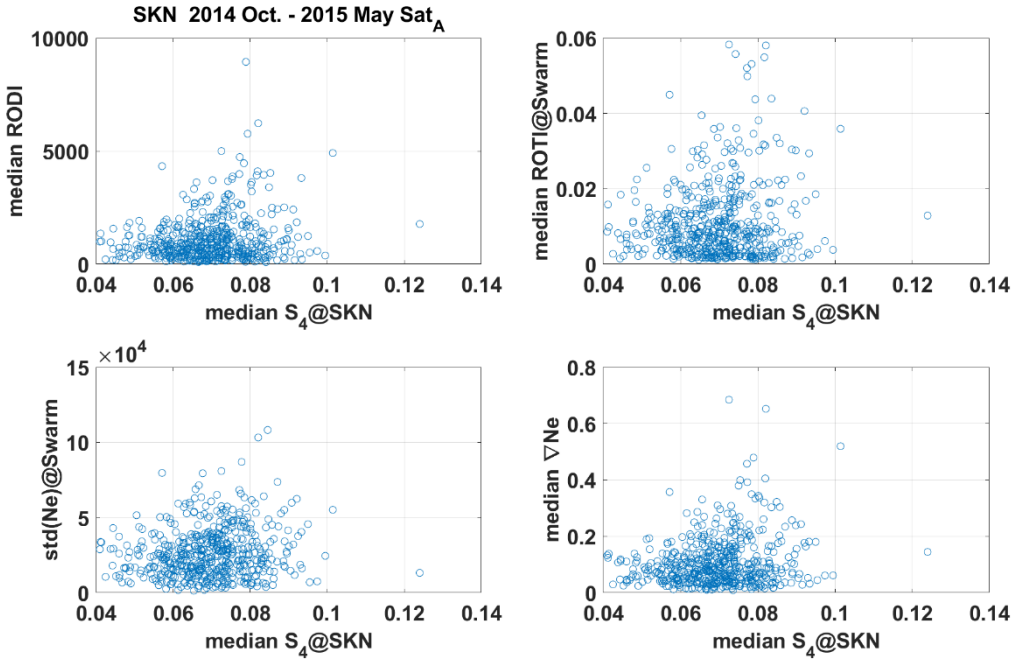

Fig. 17. The same format as Fig. 15 but for S_4.

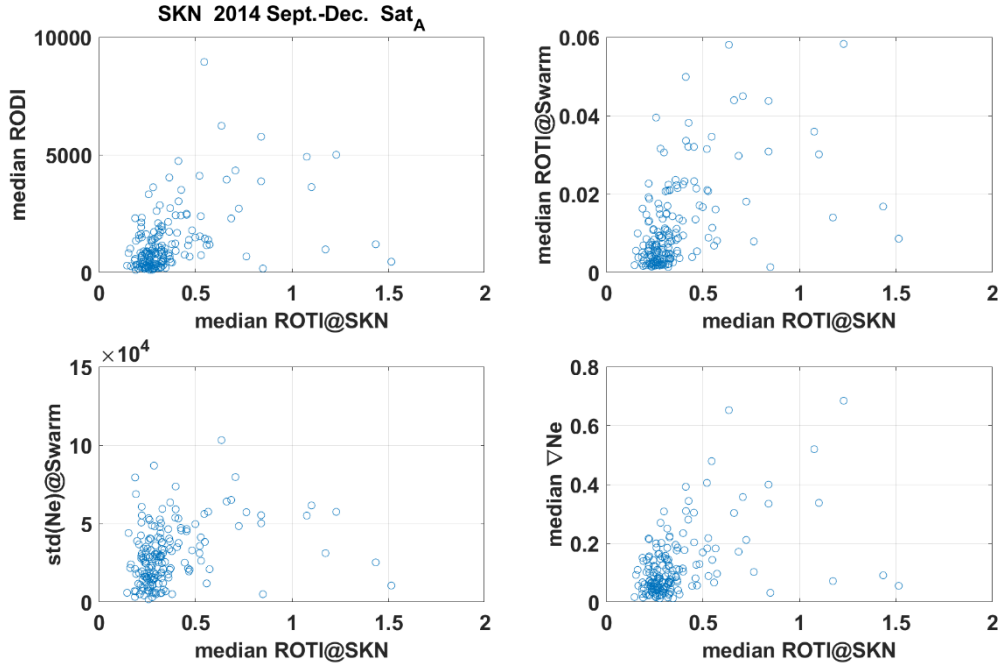

Fig. 18. The same format as Fig. 15 but for ROTI.

Analysing data from SKN station, it is evident that again for the auroral region, there is a good linear relationship between VTEC measurement on the ground and median VTEC and median Ne measured by Swarm. Better relationship between Ne and ground based TEC measurements are due to the fact that the density decreases with the altitude, and thus the local plasma density is more likely representative to the VTEC measured on the ground.

There is a non-trivial relationship between median phase and amplitude scintillation index and parameters measured at Swarm. This is due to very dynamic ionosphere conditions in the auroral region, where the median scintillation index may not be representative for the actual conditions encountered by Swarm. In addition, amplitude scintillations are not frequent at high latitudes. Finally, there is a relation between median ROTI measured at SKN and other parameters (apart from std(Ne)) at Swarm.

5.4 Conjunction with the low-latitude station at SZT (ShenZhen)

ShenZhen is a low-latitude station near the magnetic equator (see Fig. 7), where the receiver can occasionally observe equatorial plasma bubbles. Fig. 19 shows the daily plot of the GPS data from ShenZhen on Sept. 10, 2014. From 12 UT to 19 UT(20-03 LT), the GPS TEC and ROT show clear variations, and the amplitude and phase scintillation indices show clear scintillations as well. These scintillations and ROT variations are likely to be caused by plasma bubbles. In Fig. 20 we show the conjunction with Swarm A. The electron density shows a small plasma bubble (depletion in density) at around 16:36.30 UT, and the ROD, RODI, ROT, and ROTI all show significant variations with the plasma bubble.

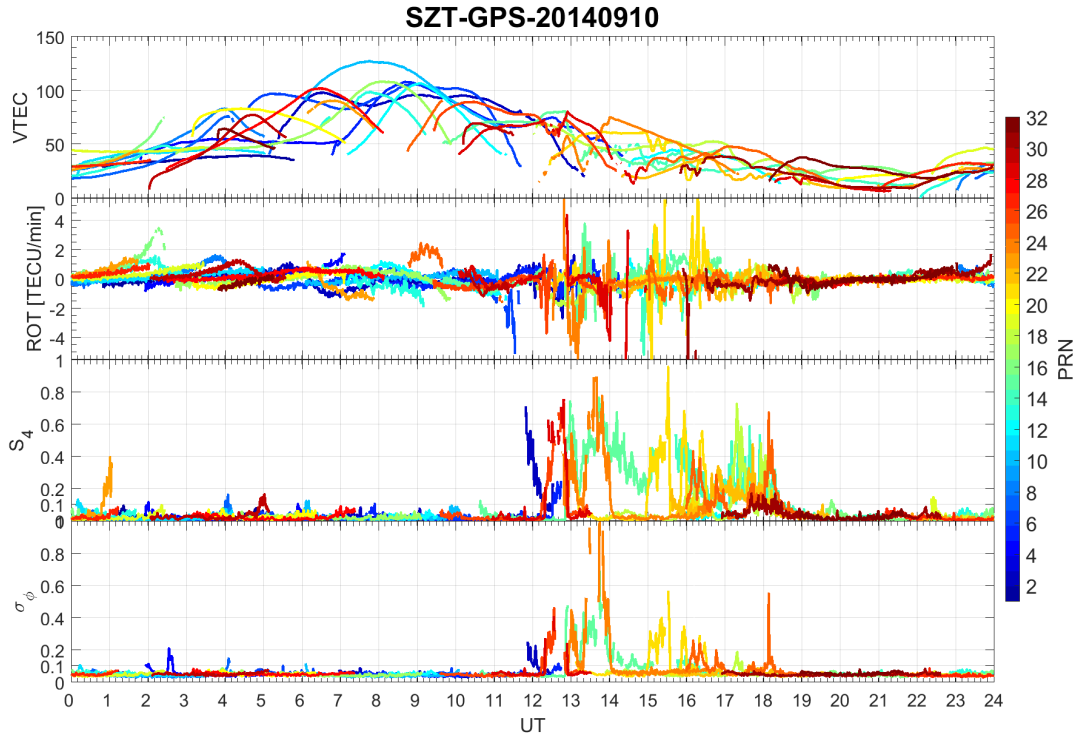

Fig. 19. Daily plot of (a) GPS TEC, (b) rate of change of TEC (ROT), (c) amplitude scintillation index (S_4), and (d) phase scintillation index (σ_ϕ) from SZT station.

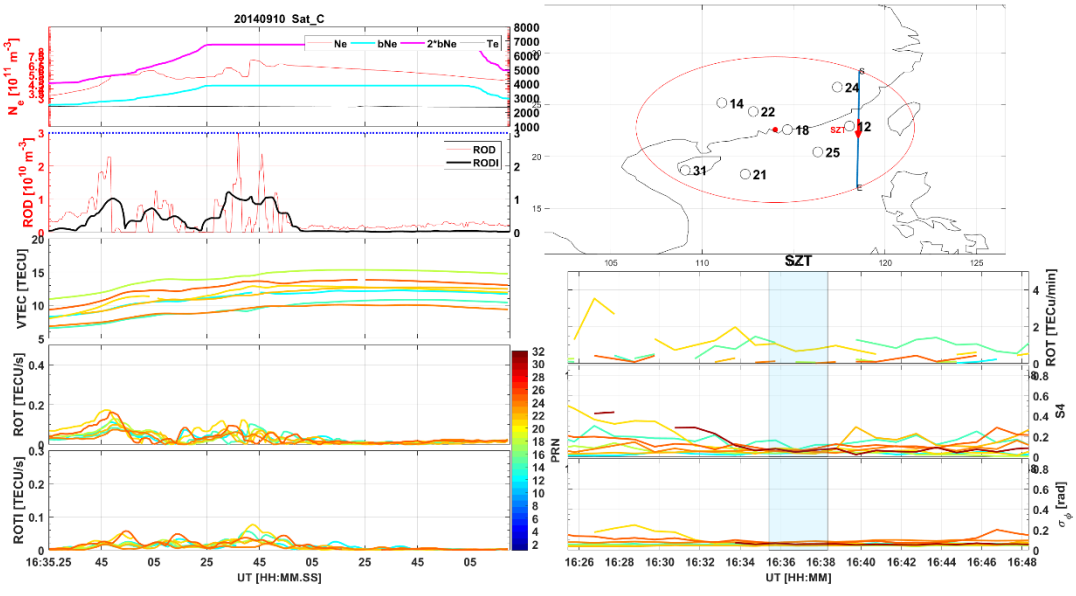

Fig. 20. An example of the conjunction of Swarm B and the ground-based GPS scintillation receiver at Shen-Zhen. The figure is in the same format as Fig. 8. The same day in Fig. 19 but for a shorter time interval.

We use the GPS data from September to December 2014 for comparison with the IPIR dataset. We only use ground-based GPS data above 30 degrees elevation angle and when the Swarm satellite passed the field-of-view for longer than 60 seconds. Fig. 21 show the scatter plot of VTEC from ShenZhen versus Ne as well as VTEC onboard Swarm. As ShenZhen is at low latitudes, there are much fewer conjunction points than

for the high-latitude Ny-Ålesund station. For this reason, we choose to plot the conjunctions with all three Swarm satellites. Due to the similar orbit characteristics for Swarm A and C, the result for these two satellites are very similar. Fig. 21 shows the strong correlation between three different datasets. It should be noted that the slopes between VTEC onboard Swarm and the VTEC from ground-based GPS receivers at ShenZhen and Ny-Ålesund are similar. However, the slopes between the in-situ *Ne* and the ground-based VTEC are quite different (9.8×10^3 at Ny-Ålesund versus at 1.9×10^4 at ShenZhen), and this is likely related to the ionospheric profile and thickness at different ionospheric regimes (polar cap vs. equatorial region). Note that *Ne* and TEC onboard Swarm B are smaller than those from Swarm A and C. This is because that Swarm B is at higher altitudes than Swarm A and C.

We also compare the four selected irregularity parameters from Swarm with the ground-based amplitude (S_4), phase scintillation (σ_ϕ) indices and ROTI in Fig. 22-24 which show loose correlation between the ground-based irregularity parameters and the space-based ones.

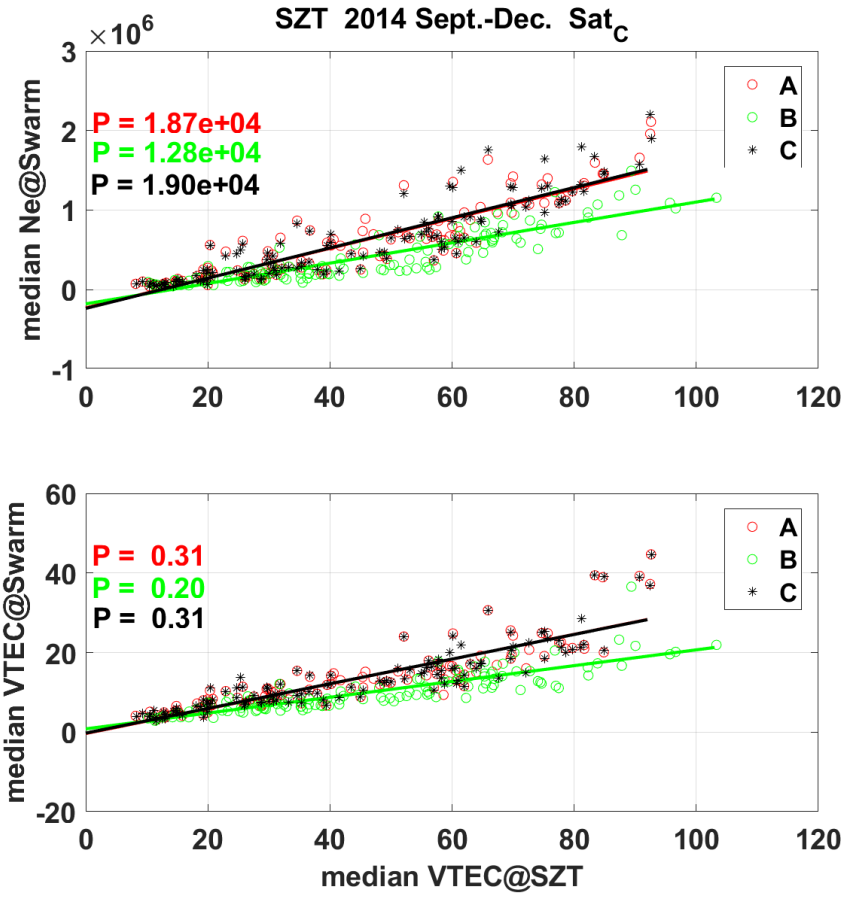

Fig. 21. Scatter plot of VTEC from SZT versus VTEC and electron density (Ne) from Swarm A. One circle in each plot represents one conjunction in Fig. 20. The results from different Swarm satellites are presented in different colors and symbols.

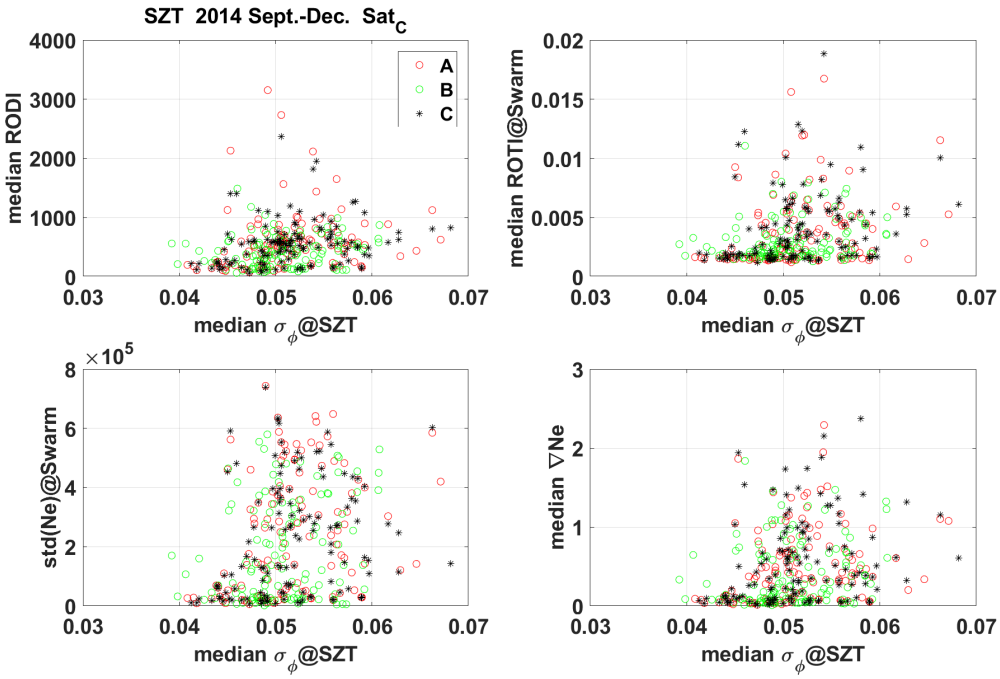

Fig. 22. Scatter plot of the phase scintillation index (σ_ϕ) from SZT versus selected parameters from Swarm A. Here one circle in each plot represents one conjunction in Fig. 20. The results from different Swarm satellites are presented in different colors and symbols.

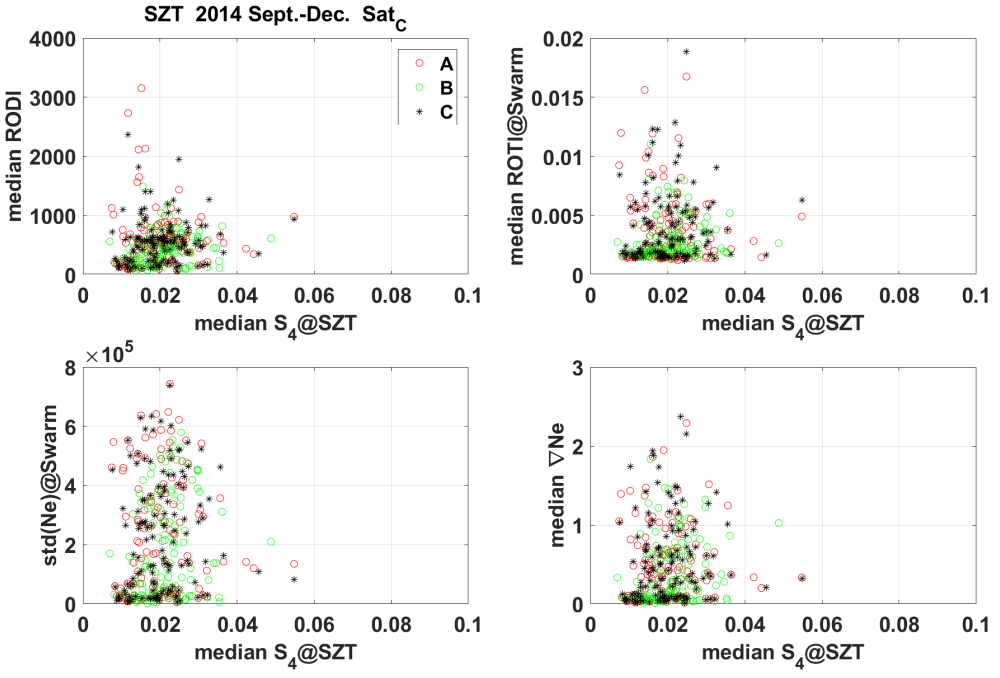

Fig. 23. The same format as Fig. 22 but for S_4.

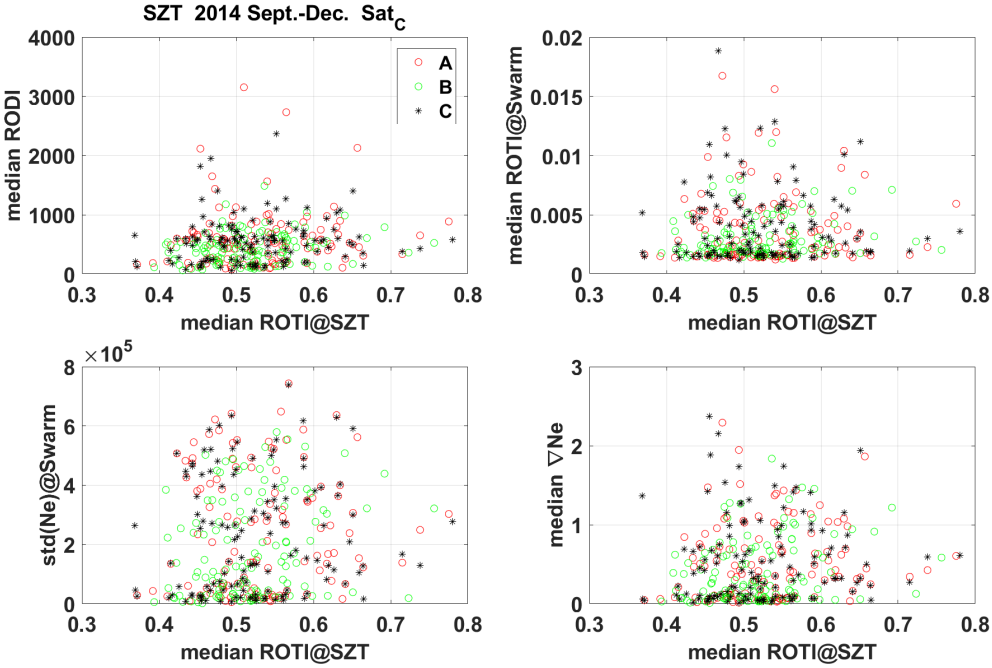

Fig. 24. The same format as Fig. 22 but for ROTI.

5.5 Determining the scale for the IPIR index ζ.

As described in [AD-5], SW-TN-UiO-GS-003, Swarm-IPIR Description of the Processing Algorithm, the IPIR index ζ provides information on the strength of ionospheric fluctuations based on their temporal variations and amplitude. In order to determine the scale of the IPIR index that would also reflect the impact of the irregularities on the trans-ionospheric radio signals, we use the ground-based scintillation data. As noted in previous sections, there is no straightforward relation between the scintillations measured on the ground and the plasma density irregularities measured in-situ by Swarm.

Fig. 25 shows the distribution of the numerical values of the IPIR index. One can notice that there are little values for $\zeta < 10^2$ $cm^{-3}s^{-1}cm^{-3}$. This result corresponds well with the long-term distribution of the Kp index (note that the IPIR index distribution is only presented for year 2015) presented in Fig. 26, confirming that the large values of ionospheric irregularities can be related to the geomagnetic disturbances.

To further investigate the latitudinal and temporal variations of the IPIR index, we plot in Fig. 27 a distribution of numerical values of ζ as a function of geomagnetic regions (equatorial, mid-latitudes, and polar regions) and day/night time for equatorial regions. It is evident that the largest values of ζ are associated with the polar regions, while the smallest correspond to the mid-latitudes, where the peak corresponds to ζ=10^4 $cm^{-3}s^{-1}cm^{-3}$. Irregularities in the equatorial regions are characterised by a double hump. Note that the total does not correspond to the sum of presented results since not all MLT are plotted for the equatorial regions.

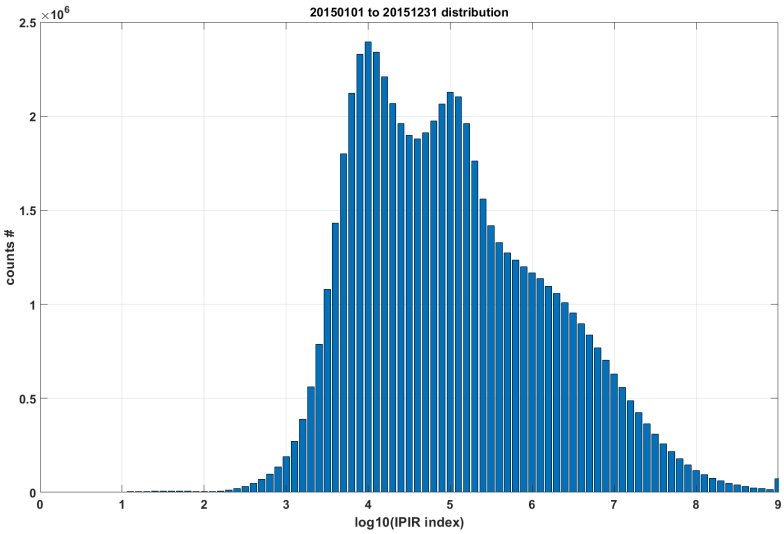

Fig. 25. Distribution of the IPIR index numerical values. The horizontal axis is logarithmic.

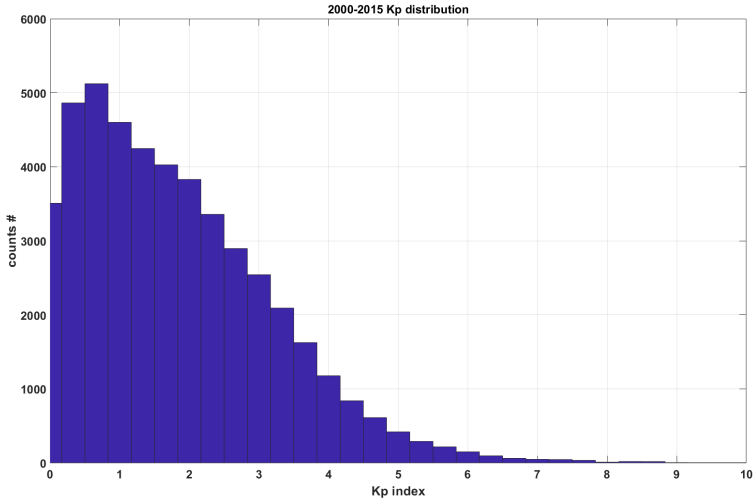

Fig. 26. Distribution of the Kp index for years 2000-2015.

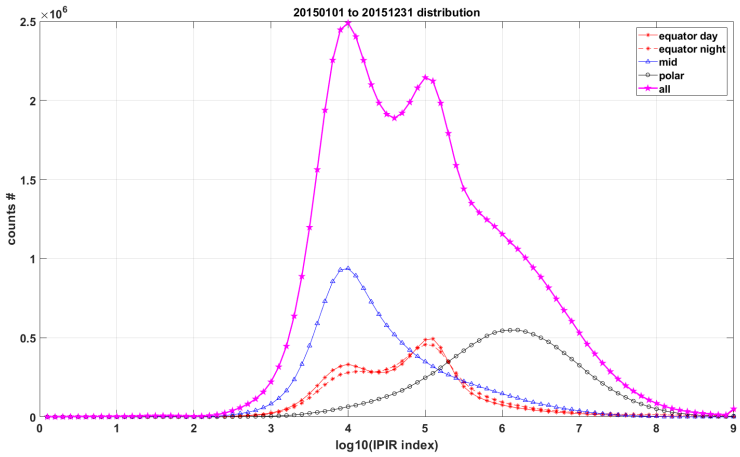

Fig. 27. Distribution of the IPIR index numerical values as a function of geomagnetic regions (equatorial, mid-latitudes, and polar regions) and day (6-15 MLT) /night (18-03 MLT) time for equatorial regions. The horizontal axis is logarithmic.

To relate the IPIR index to ionospheric scintillations, we choose to use the phase scintillations for the GNSS signals measured at the NYA station. The results are shown in Fig. 28. While there is no clear linear relationship, we do observe that the level of scintillations increases with increasing ζ. Larger ζ also relate to increase in the minimal observed scintillation levels. Thus, the likelihood of intense scintillations increases with increasing ζ. For values lower than 10^5 there is a low or very low probability of phase scintillations. Scintillations become increasingly important for numerical values of $\zeta \in (10^5\text{-}10^7)$, which we refer to a medium probability of phase scintillations. However, for values $\zeta > 10^7$ there are almost no very weak scintillations observed, while the mean level of phase scintillations increases and severe scintillations are more likely to be present. Thus, the following scale for the severity of ionospheric irregularities for the users has been established:

IPIR index scale	**Numerical value of ζ** [cm^{-3} s^{-1} cm^{-3}]	**Probability phase scintillations**
1	$< 10^3$	Insignificant
2	10^3-10^4	Low
3	10^4-10^5	Low
4	10^5-10^6	Medium
5	10^6-10^7	Medium
6	10^7-10^8	High
7	10^8-10^9	High
8	$> 10^9$	Very high

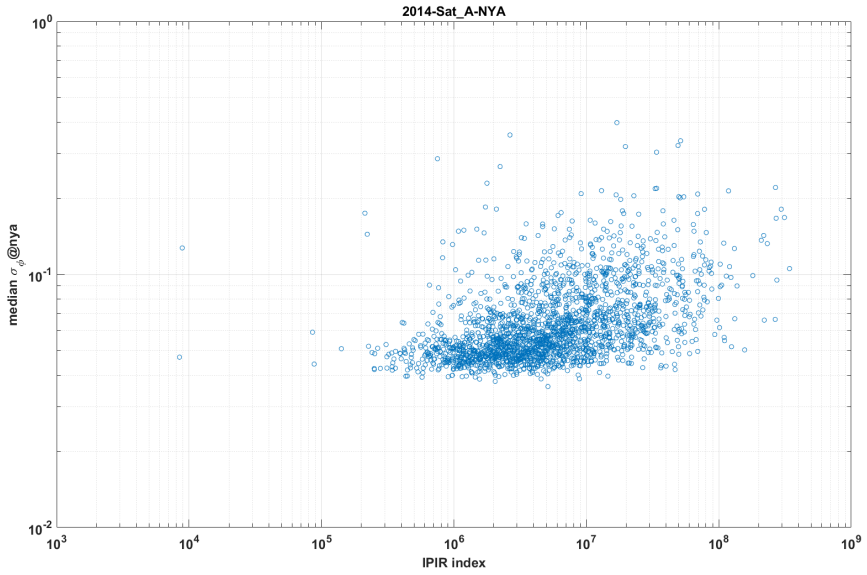

Fig. 28. Median phase scintillations at NYA as a function of the IPIR index numerical values. The axes are logarithmic.

For completeness, we also present in Fig. 28 the corresponding data for stations Skibotn and ShenZhen. Results from Skibotn agree well with Ny-Alesund. While for ShenZhen, a limited number of data points due to limited conjunctions and infrequent scintillations makes it difficult to draw firm conclusions, this station still shows a weak trend of stronger scintillations with increasing IPIR index. As the IPIR index is intended to be a global product, the use of the polar stations for determining the scale is justified based on the global and local distributions as shown in Figs. 25 and 27.

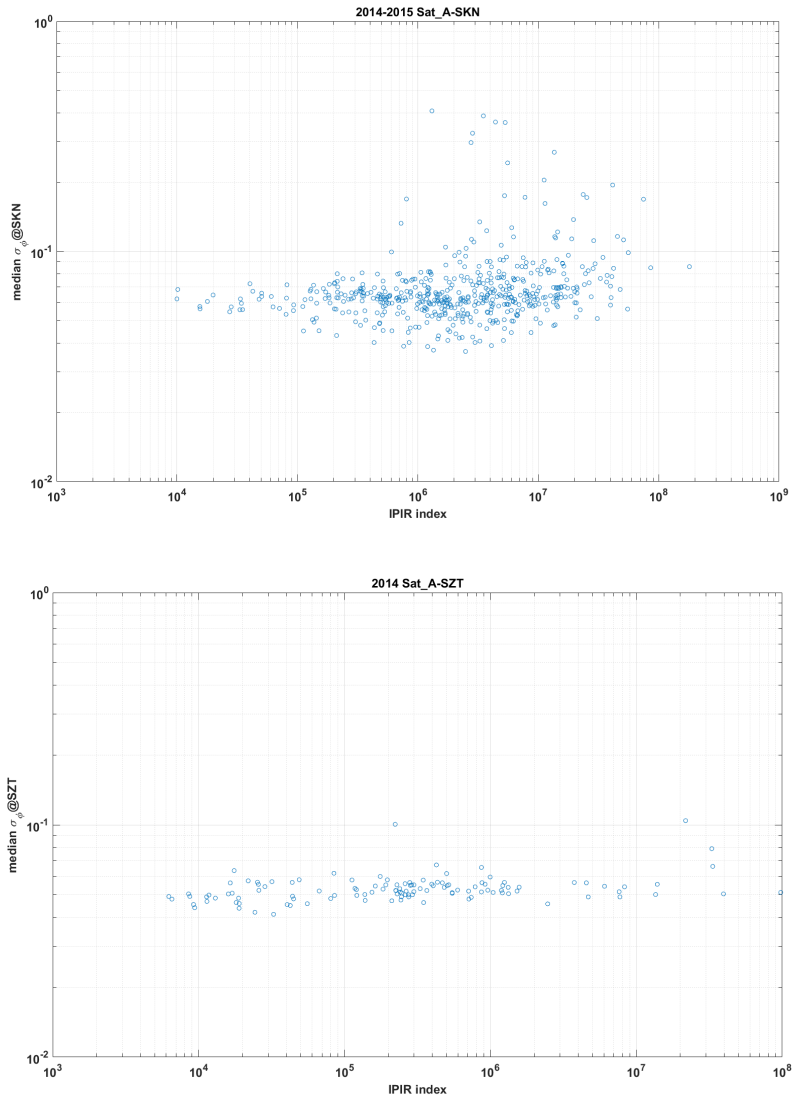

Fig. 29. Median phase scintillations at SKN (top) and SZT (bottom) as a function of the IPIR index numerical values. The axes are logarithmic.

6 Discussion and conclusions

There is a very good agreement between the Swarm based measurements of TEC and electron density. The fluctuations in the electron density and TEC are correlated, and the correlation in RODI and ROTI is good during active conditions, i.e., when irregularities in the plasma density are present. This supports the use of two datasets for characterising ionospheric plasma irregularities in-situ by Swarm.

There is a good agreement between the median VTEC measured by the ground-based GISTM receivers at all considered geomagnetic latitudes and the VTEC as well as electron density measured by Swarm. There is a better linear relationship between the VTEC measured by ground receivers and the electron density measured by Swarm. This is because VTEC measurements from the ground include the actual density values corresponding to the Swarm orbit, while VTEC measured by Swarm only accounts for electron densities above the satellites.

The relationship between scintillation indices measured with the ground receivers and parameters derived from Swarm measurements is nonlinear, which is as expected. Scintillations are the effect of scattering and diffraction of waves in the irregular medium, and in case of the amplitude scintillations, these irregularities are of the order of hundreds of meters, while Swarm can measure gradients at scales larger than several kilometres. Furthermore, the scattering and interference is not a linear function of irregularities, but a result of those. Nevertheless, we do expect an increase of scintillations with the geomagnetic activity and the strength of irregularities, albeit not necessarily linear. Detailed comparison of the phase scintillation indices with the IPIR index reveals an increase in the mean phase scintillation index values with increasing IPIR index. At the same time the likelihood of large scintillations increases as well. This allows to relate the strength ionospheric plasma irregularities as reflected in the IPIR index to the impact on transionospheric radio signals and severity of plasma irregularities for the end-users. Since IPIR index is a global product, we choose the high latitude station to establish its scale.

There is a near-linear relation between the ground-based measurements for ROTI and the Swarm measurements of ROTI and RODI and variations in the electron density. This relation is very good at high latitudes, but not that clear at mid-latitudes. This can be attributed to the geometry of the Earth magnetic field. Plasma density variations extend along the magnetic field lines and thus it is more likely that variations observed by the ground-based receivers are also experienced similarly by a satellite at high geomagnetic latitudes. At low latitudes, the variations in density can be within a horizontal layer above or below satellite.

To conclude, we compared the GPS data measured with the ground-based receivers with the IPIR datasets, and in particular new quantities. We selected three ground stations to present the different ionospheric regions, i.e., polar cap station at Ny-Ålesund (NYA), auroral station at Skibotn (SKN), and equatorial station in ShenZhen (SZT).

1. Data for ground-based VTEC from all stations considered shows good linear relation with in-situ electron density and VTEC onboard Swarm.
2. The relation between the ground-based scintillation indices (S_4 and σ_ϕ) and the Swarm derived irregularity parameters is not straightforward since scintillations are the indirect result of irregularities, however we observe an increase in scintillations with an increase in ionospheric plasma disturbances.
3. The increase in scintillations with increasing plasma irregularities as reflected in the IPIR index allows us to establish the scale for the IPIR index which reflects the severity of the fluctuations from the user perspective in a statistical sense, indicating the likelihood of scintillations of trans-ionospheric radio signals.

***Acknowledgment**: We thank the Norwegian Polar Institute for assisting in GPS observations at Ny-Ålesund, and the Tromsø Geophysical Observatory for operating the receiver at Skibotn. Yaqi Jin thanks Prof. DongHe Zhang for providing GPS data from ShenZhen.*